Chemical Engineering Journal 150 (2009) 261–268

Contents lists available at ScienceDirect

Chemical Engineering Journal

journal homepage: www.elsevier.com/locate/cej

Al content dependence of reaction behaviors and mechanism in combustion synthesis of TiB_2–AlN-based composites

Ping Shen*, Weihua Sun, Binglin Zou, Lei Zhan, Qichuan Jiang

Key Laboratory of Automobile Materials, Ministry of Education, and College of Materials Science and Engineering, Jilin University, No. 5988 Renmin Street, Changchun 130025, PR China

ARTICLE INFO

Article history:
Received 17 November 2008
Received in revised form 13 February 2009
Accepted 19 February 2009

Keywords:
Ceramic matrix composites
Self-propagating high-temperature synthesis (SHS)
Microstructure
Reaction mechanism

ABSTRACT

The TiB_2–AlN and TiB_2–AlN–TiN ceramic matrix composites were successfully produced by self-propagating high-temperature synthesis (SHS) reactions from the Al–Ti–BN compacts through the manipulation of the Al reactant content. The effects of the Al content on the adiabatic and practical maximum combustion temperatures, wave velocity, phase composition and microstructure of the synthesized products, and reaction mechanism were investigated in detail. Thermodynamically and practically, the reaction was most exothermic for the Al content being 35.5 wt.% in the reactants to produce only the dual TiB_2–AlN phases. Kinetically, the reaction commenced with the formation of Al_3Ti, and then proceeded with the interactions of the Al–Ti intermetallics/melts with BN to yield the AlN and TiB_2 phases. The substantial reaction between the elemental Ti and BN into formation of TiN took place only in the low Al content samples. On the other hand, the presence of considerable amount of the TiN grains effectively inhibited the abnormal growth of the TiB_2 grains, leading to very fine microstructures; whereas, the grain growth of TiB_2 and AlN as well as their inhomogeneous distribution was enhanced by the increase in the Al reactant, while TiN was completely inhibited from development.

1. Introduction

Titanium diboride and nitride (TiB_2 and TiN) have received increasing attention due to their unique properties such as high melting point, high hardness, good electrical conductivity, high chemical and thermal stability, and excellent wear and corrosion resistance [1,2]. Aluminum nitride (AlN) is another attractive ceramic with high melting point, low thermal expansion coefficient, excellent electrical insulation, high heat conductivity, and high strength at room temperature [3,4]. Combination of these ceramics was reported to further improve their properties and/or to offset their weakness, *e.g.*, the presence of TiN in the TiB_2 matrix could effectively inhibit the anisotropic growth of the TiB_2 grains and improve the corrosion resistance to HCl [5], while the addition of TiB_2 to TiN has the potential of improving the hardness and toughness of TiN [6,7]; on the other hand, the addition of a small amount of AlN to TiB_2 considerably enhances its sintering densification without deterioration of properties [8]. Such advantageous characteristics or superior properties make their composites more attractive for applications as advanced structural materials.

Conventionally, fabrication of these ceramic matrix composites requires complicated and expensive hot-pressing or hot isostatic pressing techniques [9,10]. Long exposures at high temperatures during sintering not only increase the production cost but also result in the coarsening of microstructure. Self-propagating high-temperature synthesis (SHS), also termed combustion synthesis or reaction synthesis, is a good method for producing advanced ceramic composites with fine microstructures using relatively cheap and abundant precursors [2,4,5,7,11,12]. For instance, Yeh and Teng [2] prepared the TiN–TiB_2 composites using compacted samples of titanium (Ti) and boron nitride (BN) powders ignited in gaseous nitrogen and investigated the effect of sample green density, nitrogen pressure, starting stoichiometry of reactant compacts and TiN diluent content on the degree of conversion and combustion characteristics. Tomoshige et al. [5] fabricated the TiB_2–TiN composites with various compositions by the similar method using the Ti, B and BN as raw materials. Zhang and Jin [11] produced the TiB_2–2AlN-based composites by reactive hot-pressing using mixtures of Al, Ti and BN in a molar ratio of 2:1:2 and examined the phase formation mechanism through firing the mixtures at temperatures between 1273 and 2013 K for 30 min and then cooling down for X-ray diffraction (XRD) analysis. They suggested the following reaction steps:

$$3Al + Ti \rightarrow Al_3Ti, \quad (1)$$

* Corresponding author. Tel.: +86 431 8509 4699; fax: +86 431 8509 4699.
E-mail address: shenping@jlu.edu.cn (P. Shen).

1385-8947/$ – see front matter © 2009 Elsevier B.V. All rights reserved.
doi:10.1016/j.cej.2009.02.029

$$3Ti + 2BN \rightarrow TiB_2 + 2TiN, \quad (2)$$

$$3TiN + Al_3Ti \rightarrow 3AlN + 4Ti. \quad (3)$$

Gutmanas and Gotman [12], on the other hand, considered more complicated reactions in the Al–Ti–BN systems by varying the reactant stoichiometry and suggested the following overall reaction:

$$m(2BN + 3Ti) + n(2BN + 3Al) \rightarrow mTiB_2 + 2mTiN + nAlB_2 + 2nAlN. \quad (4)$$

They further argued theoretically that, depending on the m/n ratio, products with different phase compositions should be obtained. For $m/n > 0.5$, *i.e.*, high Ti contents in the starting blend, a fully ceramic TiB_2–TiN–AlN product would be produced according to the reaction:

$$m(2BN + 3Ti) + n(2BN + 3Al) \rightarrow (m+n)TiB_2 + (2m-n)TiN + 3nAlN. \quad (5)$$

For $m/n = 0.5$, *i.e.*, Al:Ti:BN = 2:1:2 in molar ratio, the most thermodynamically feasible reaction would result in the formation of only TiB_2 and AlN according to:

$$(2BN + 3Ti) + 2(2BN + 3Al) \rightarrow 3TiB_2 + 6AlN. \quad (6)$$

For $m/n < 0.5$ or $n/m > 2$, *i.e.*, high Al contents in the blend, the final product consisting of TiB_2, AlN and AlB_2 may be synthesized according to the reaction:

$$m(2BN + 3Ti) + n(2BN + 3Al) \rightarrow 3mTiB_2 + 2(m+n)AlN + 2(n-2m)AlB_2. \quad (7)$$

An experimental validation of the above reactions, however, was performed only for one composition of 6Al–3Ti–6BN ($n/m = 2$) using a thermal explosion technique and the final reaction product consisted of TiB_2, AlN and a considerable amount of Al_3Ti, which was in general agreement with the theoretical prediction.

As indicated, the reactions in the Al–Ti–BN system seem quite complicated mainly because of the reactant content dependence of the competitive reactions for formation of TiN and AlN. In this study, we investigated the reaction behaviors and mechanisms in the SHS reactions of the Al–Ti–BN compacts containing different Al reactant contents with a purpose to provide helpful guidance for better control of the reaction process and achievement of the desirable products with tailored microstructures in our future work for producing the dense TiB_2–AlN-based composites.

2. Experimental procedure

The starting materials were commercial powders of 99 wt.% Al (Northeast light alloy Ltd. Co., Harbin, China) with an average particle size of 29 μm, 99.5 wt.% Ti (Institute of Nonferrous Metals, Beijing, China) with particle sizes of 25–48 μm, and 99 wt.% BN (Ying Kou liaobin Fine Chemicals Co. Ltd., Liaoning, China) with an average particle size of 3 μm, except for the case in combustion wave quenching experiments, where much coarser BN particles (~75 μm) were used. To avoid great variety and complexity, the molar proportion of Ti to BN was fixed to 1:2 in this study. The Al content varied from 10 to 60.5 wt.% of the total weight of the reactants. Depending on the Al content, the reactions were assumed to evolve as follows:

(1) For the Al content being higher than 35.5 wt.% (*i.e.*, >40 mol.%),

$$(x+2)Al + Ti + 2BN \rightarrow TiB_2 + 2AlN + xAl. \quad (8)$$

(2) For the Al content being less then 35.5 wt.%,

$$y(2Al + Ti + 2BN) + 3Ti + 6BN \rightarrow 2yAlN + 2TiN + (y+1)TiB_2 + 4BN. \quad (9)$$

In case (2), because of the constraint of Ti:BN (1:2 in molar ratio), BN would be excessive in the reactants and the excess part was expected to act as diluent during combustion reaction.

The reactant powders with proper weights were first wet-mixed in an alumina mortar by adding a suitable proportion of acetone for 20 min, roasting at 373 K for 10 min and then dry-mixed for 30 min to ensure homogeneity. The powder mixtures were then uniaxially pressed into cylindrical compacts of ~22 mm in diameter and ~15 mm in height with green densities of 70 ± 3% of theoretical, as determined from weight and geometric measurements.

The SHS experiments were performed in a stainless steel glove box in Ar (99.9% purity) atmosphere at a pressure of 0.1 MPa, as described in detail elsewhere [13]. The compact was ignited by arc heating a thin graphite plate (~2.5 mm), on which the sample was preplaced, using a current of 60 A and a voltage of ~220 V. The combustion temperature was measured by W5–Re26 thermocouples, which were enclosed in fine alumina tubes to protect from reaction with the reactants at elevated temperatures and pre-located in a small hole in close vicinity to the center of the compact. The signals were recorded and processed by a data acquisition system using an acquisition speed of 50 ms/point. The combustion process was recorded by a CCD video camera using a scanning speed of ~34 frames/s to evaluate the wave propagation velocity. The phase compositions in the reacted samples were identified by XRD (Rigaku D/Max 2500PC, Tokyo, Japan) and the microstructures were examined by scanning electron microscopy (SEM, JSM 5310, Tokyo, Japan) and field emission SEM (FESEM, JSM 6700F, Tokyo, Japan).

In order to clarify the reaction sequence and phase formation mechanism, the copper-mold-aided combustion-wave-front quenching experiments (a schematic illustration and more detailed description were presented in Ref. [14]) were carried out for the samples with different Al contents (10, 25, 35.5 and 45 wt.%) using coarser BN powders (~75 μm), which favors the realization of quenching. The phases in the differently reacted regions of the quenched samples were identified by an X-ray microdiffractometer (D8 Discover with GADDS, Bruker AXS, Karlsruhe, Germany) using an 800 μm beam diameter and microstructures were examined by SEM coupled with energy dispersive X-ray spectrometry (EDS, Link-ISIS, Oxford, England) analysis.

3. Results and discussion

3.1. Adiabatic combustion temperatures

The adiabatic combustion temperature (T_{ad}) is a good measure of the exothermicity of the reaction and the state of the various phases. Providing the self-propagating mode was initiated at room temperature (298 K) without any preheat, the values of T_{ad} for reactions (8) and (9) could be calculated using thermodynamic data in Refs. [15,16] based on the following equation [17],

$$\Delta H(298) + \int_{298}^{T_{ad}(298)} \sum n_j C_P(P_j) dT + \sum_{298-T_{ad}(298)} n_j L(P_j) = 0 \quad (10)$$

where $\Delta H(298)$ is the reaction enthalpy at 298 K, n_j is the stoichiometric coefficient of the product, $C_P(P_j)$ and $L(P_j)$ are the heat capacity and latent heat (if the product goes through a phase change, *e.g.*, solid to liquid or liquid to gas) of the product, respectively. The Al reactant content dependence of the *postulated* reaction products [based on Eqs. (8) and (9)] and the calculated T_{ad} is shown

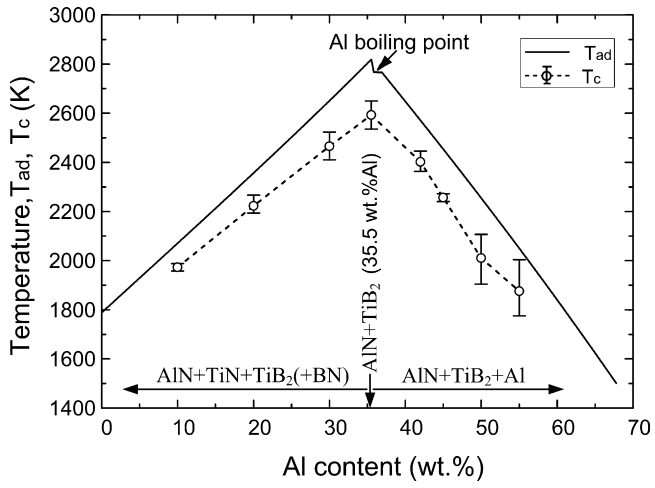

Fig. 1. Variations in theoretically calculated adiabatic temperature (T_{ad}) and experimentally determined maximum combustion temperature (T_c) as well as the postulated reaction product with the Al content in the reactants (in weight percent).

in Fig. 1, together with the experimentally determined maximum combustion temperatures (T_c). As can be seen, the adiabatic temperature increases with increasing Al content, reaching a maximum (2817 K) at 35.5 wt.% Al, and then decreases with further increase in the Al content, suggesting that the reaction for the formation of only the TiB_2 and AlN ceramics is most exothermic in the Al–Ti–BN system.

3.2. Changes in standard Gibbs free energy and reaction enthalpy

Fig. 2(a) and (b), respectively, show the changes in the standard Gibbs free energy (ΔG°) and reaction enthalpy (ΔH°) using the thermodynamic data in Refs. [15,16] for the following potential reactions betweens the reactants in the Al–Ti–BN system as well as between the reactants and some intermediate phases:

$$3/4Al + 1/4Ti \rightarrow 1/4Al_3Ti \quad (11)$$

$$3/5Al + 2/5BN \rightarrow 1/5AlB_2 + 2/5AlN \quad (12)$$

$$1/2AlB_2 + 1/2Ti \rightarrow 1/2TiB_2 + 1/2Al \quad (13)$$

$$3/5Ti + 2/5BN \rightarrow 1/5TiB_2 + 2/5TiN \quad (14)$$

$$1/2Al + 1/2TiN \rightarrow 1/2Ti + 1/2AlN \quad (15)$$

$$4/5Al + 1/5TiN \rightarrow 1/5Al_3Ti + 1/5AlN \quad (16)$$

$$1/2Ti + 1/2AlN \rightarrow 1/2Al + 1/2TiN \quad (17)$$

$$4/7Ti + 3/7AlN \rightarrow 1/7Al_3Ti + 3/7TiN \quad (18)$$

$$1/3Al_3Ti + 2/3BN \rightarrow 1/3TiB_2 + 2/3AlN + 1/3AL \quad (19)$$

As can be seen, firstly, all the reactions, except for reaction (15), seem to be thermodynamically favorable ($\Delta G^\circ < 0$) and exothermic ($\Delta H^\circ < 0$) in the calculated temperature ranges, and the ceramic phases, AlN, TiN and TiB_2, possess higher stability than the intermetallic phases such as Al_3Ti and AlB_2, implying that, if these intermetallic phases are formed in the combustion process, they should be thermodynamically driven to transform to the more stable ceramic phases. Secondly, although reaction (15), from the viewpoint of thermodynamics, is unable to proceed, reaction (16) is feasible, suggesting that in the case of presence of excess Al in the reactants, TiN would be likely to transform to AlN along with the formation of Al_3Ti. On the other hand, both reactions (17) and (18) are thermodynamically feasible, suggesting that in the case of Ti-rich, AlN might transform to TiN as well. Namely, the stability of AlN and TiN is primarily dependent on the relative contents of Al and Ti in the reactants. Finally, as compared with the others, reactions (14) and (19) possess larger thermodynamic driving force to take place. Also, they are highly exothermic, as indicated in Fig. 2(b). However, it should be pointed out that the thermodynamic conditions are only necessary but insufficient in determining the occurrence of a practical reaction. Kinetic conditions, such as concentration and the melting state of the reactive components, also play an important role in this aspect, as demonstrated later.

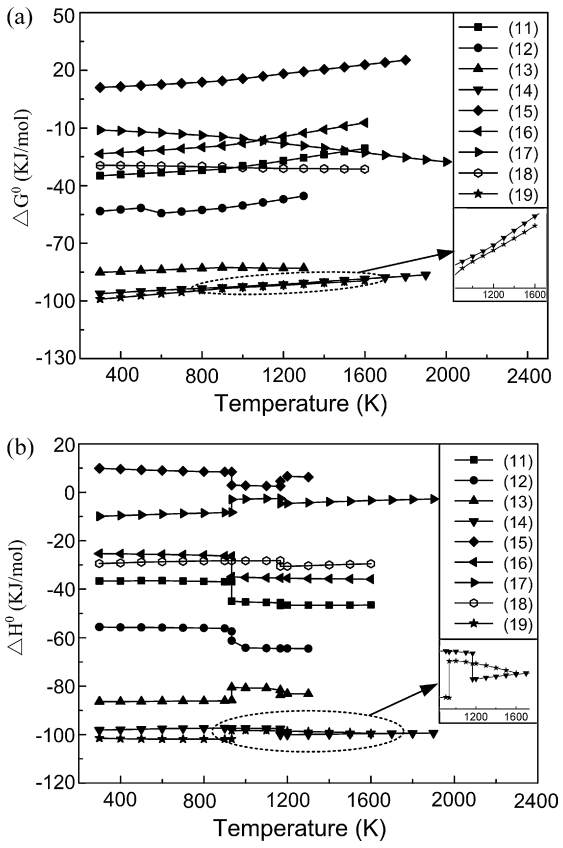

Fig. 2. Changes in (a) standard Gibbs free energy (ΔG°) and (b) reaction enthalpy (ΔH°) for reactions (11)–(19).

3.3. Reaction behaviors and products

The variation in the maximum combustion temperature (T_c) with the Al content is shown in Fig. 1 for a better comparison with T_{ad}. Clearly, T_c shows a similar variation behavior as T_{ad}, despite some (100–200 K) discrepancies in their values due to heat loss in the practical reactions. The self-sustaining reaction, on the other hand, was found difficult to initiate in the samples containing 60.5 wt.% Al in the reactants, unless a persistent arc heating was supplied.

Fig. 3 shows the variation in the combustion wave velocity with the Al content. Similar to the combustion temperature, the velocity first increased, reaching a maximum at 35.5 wt.% Al, and then decreased with increasing Al content. Such a synchronous variation reflects the fact that the combustion temperature played a significant role in affecting the wave velocity. On the other hand, it was noted that the wave velocity in the 30 wt.% Al samples was smaller than that in the 42 wt.% Al samples, yet the value of T_c was larger, and so is the case in the 20 wt.% Al samples. This exceptional behavior could be explained by the influence of thermal conductivity of the compacts. Apparently, higher thermal conductivity of the compact would favor a faster propagation of the combustion wave. In this system, the higher amount of Al increased the metal

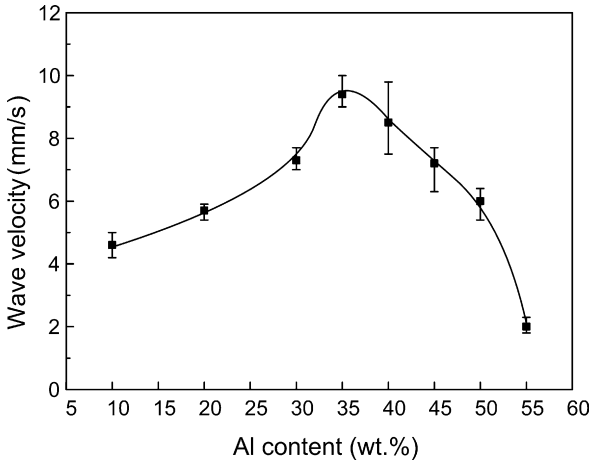

Fig. 3. Variation in the combustion wave velocity with the reactant Al content.

phase in the compact, and more importantly, the rapid melting and spreading of Al filled the pores in front of the combustion wave, thus accelerating the propagation of the combustion wave.

Fig. 4 shows the XRD patterns of the reaction products in the samples with different amounts of the Al reactant. It is clear that the reaction product depends on the Al content. For the Al content being smaller than 35.5 wt.%, the reaction products consisted of TiB_2, AlN, TiN and excess BN. For the Al content being larger than 35.5 wt.%, the products consisted of TiB_2, AlN, excess Al and a very small quantity of Al_3Ti, without TiN in the scope of the XRD detection accuracy. The formation of these products is in good agreement with the prediction indicated in Fig. 1. However, for the Al content being exactly 35.5 wt.%, in addition to TiB_2 and AlN, a small amount of TiN was found. The presence of TiN in the final product is presumed to be a result of Al evaporation at extremely high temperatures ($T_c = 2593 \pm 57$ K), leading to the Al deficiency. In this sense, the content of the Al reactant is suggested to be slightly over 35.5 wt.% in order to obtain a desirable composite consisting of only TiB_2 and AlN ceramics. On the other hand, the reaction products obtained in this study are more ideal (*i.e.*, closer to the theoretical predictions) than those reported by Zhang and Jin [11] and Gutmanas and Gotman [12] using reactive hot-pressing and thermal explosion techniques, respectively, as we have described before, suggesting that the SHS method is more favorable to produce the desirable products.

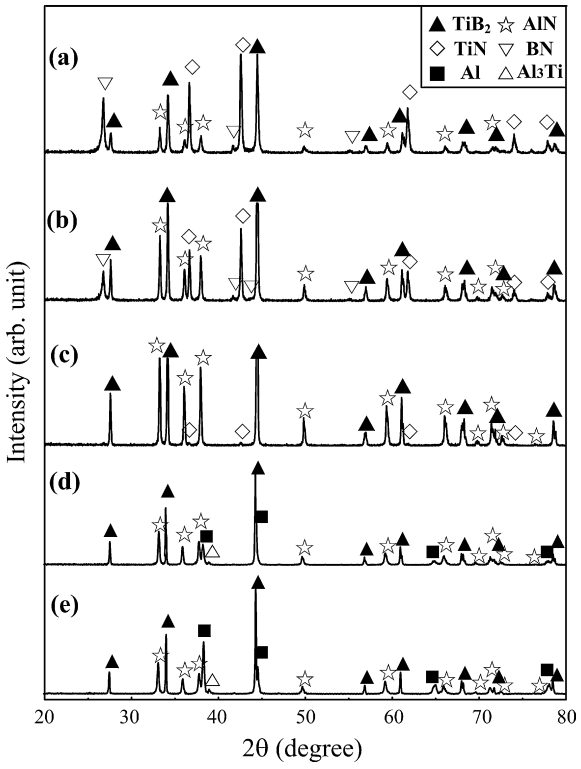

Fig. 4. XRD patterns of the combustion-synthesized products for the Al–Ti–BN samples with different amounts of the Al reactant: (a) 10 wt.% Al, (b) 20 wt.% Al, (c) 35.5 wt.% Al, (d) 45 wt.% Al, and (e) 55 wt.% Al.

Fig. 5 shows the representative FESEM images of the microstructures at the fracture surfaces of the reacted samples with different amounts of the Al reactant. The bright phases in back-scattered electron (BSE) mode are TiN and TiB_2, and the gray one is AlN. In the samples with relatively low Al contents (<35.5 wt.%), it is somewhat difficult to distinguish between TiN and TiB_2 from their morphologies. Previous studies [13,18] informed us that TiB_2 usually exhibited an abnormal grain growth with typical hexagonal prism shapes, but this was not the case in the current study. The TiB_2 grains were in fine platelet shapes with a certain degree of agglomeration, as indicated in the inset of Fig. 5(b). They seemed to intermix with the equiaxed TiN grains (possibly the brightest phase) and thus their abnormal grain growth was substantially inhibited. The characteristic grain sizes of these ceramic (AlN, TiN and TiB_2) phases were within 100–500 nm. Such fine microstructures could be attributed to competitive nucleation and growth of the ceramic grains as well as to the low amount of liquid during the SHS reactions, which provided limited space for the grain growth. With the increase in the Al content, the grains, especially for TiB_2, had a considerable extent of growth. As indicated in Fig. 5(d) and (e), the TiB_2 grains grew to 1–3 μm and their morphologies returned to the typical hexagonal prisms with larger or smaller defects such as hollows in their bodies. The equiaxed AlN grains grew to approximately 500–800 nm and were relatively homogeneous in size [Fig. 5(f)]. It was speculated that for the Al content being no more than 35.5 wt.%, the grain growth with increasing Al content could be attributed to the increase in the combustion temperature, as indicated in Fig. 1. However, for the Al content being higher than 35.5 wt.%, the combustion temperature decreased with further increase in Al, and the growth of the TiB_2 and AlN grains should be related to the increasing amount of liquid, which provided sufficient space for the grain growth and allowed the Ostwald ripening of the grains. On the other hand, it was noted that the TiB_2 and AlN grains, particularly in the high Al content samples, were distributed in separate regions, as shown in Fig. 5(d)–(f). Similar microstructures were also observed in the TiC–TiB_2/Al composites synthesized from Al–Ti–B_4C reactants and explained by the fact that the dissociation rate of carbon from the B_4C crystal and its diffusion rate in the Al–Ti melt were much larger than those of boron [19]. According to Ref. [20], the diffusion rate of C in β-Ti is approximately three orders of magnitude higher than that of B at 1473 K; whereas the diffusion rate of C in β-Ti is no more than one order of magnitude higher than that of N in the temperature range of 1473–1873 K [21]. Therefore, it can be inferred that the diffusion rate of N is much faster than that of B. On the other hand, the solubility of N in liquid Al is small, while that of B in liquid Al and Ti as well as N in liquid Ti is quite large at high temperatures [22]. Therefore, AlN would preferentially precipitate from the Al–Ti melt and the higher Al content favors a larger amount of the AlN precipitation, leading to the enhanced separate distribution of the AlN and TiB_2 grains.

3.4. Reaction mechanisms

To reveal the reaction mechanisms in the Al–Ti–BN system and the effect of the Al content, the Cu mold-aided combustion wave

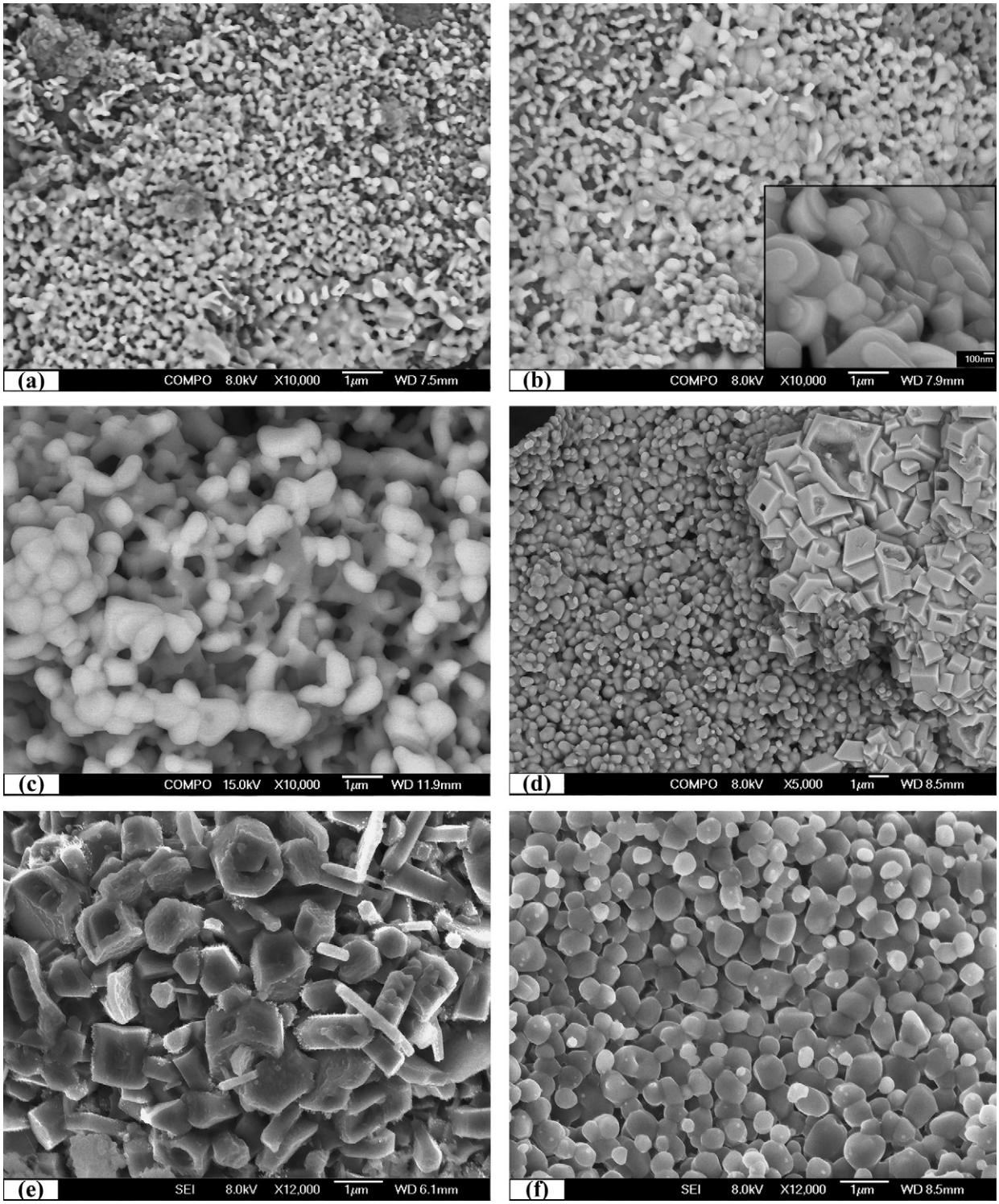

Fig. 5. Representative FESEM images of the microstructures at the fracture surfaces of the combustion-synthesized samples with different amounts of the Al reactant: (a) 10 wt.% Al, (b) 20 wt.% Al, (c) 35.5 wt.% Al, (d) 45 wt.% Al, and (e) and (f) 55 wt.% Al. Figures (a)–(d) are in back-scattered electron (BSE) mode and figures (e) and (f) in second electron (SE) mode.

quenching experiments were performed for the samples containing 10, 25, 35.5 and 45 wt.% Al. Figs. 6 and 7, respectively, show the X-ray microdiffraction patterns of the phases in different regions of the representative 45 and 25 wt.% Al–Ti–BN samples. The former stands for the Al-rich case and the latter for the Al-deficient case. It is worth mentioning that the phase evolution history in the samples with 10 and 35.5 wt.% Al was similar to that in the 25 wt.% Al sample, except for the variation in relative intensities of various phases due to the difference in the proportion of the reactants, and thus it was not presented here.

According to Fig. 6, the phase evolution history in the 45 wt.% Al–Ti–BN sample could be described as:

$$(a)Al + Ti + BN \rightarrow (b)Al + Ti + BN + Al_3Ti \rightarrow (c\text{–}d)Al + Ti + BN + Al_3Ti + AlN + TiB_2 \rightarrow (e)Al + BN + Al_3Ti + AlN + TiB_2$$

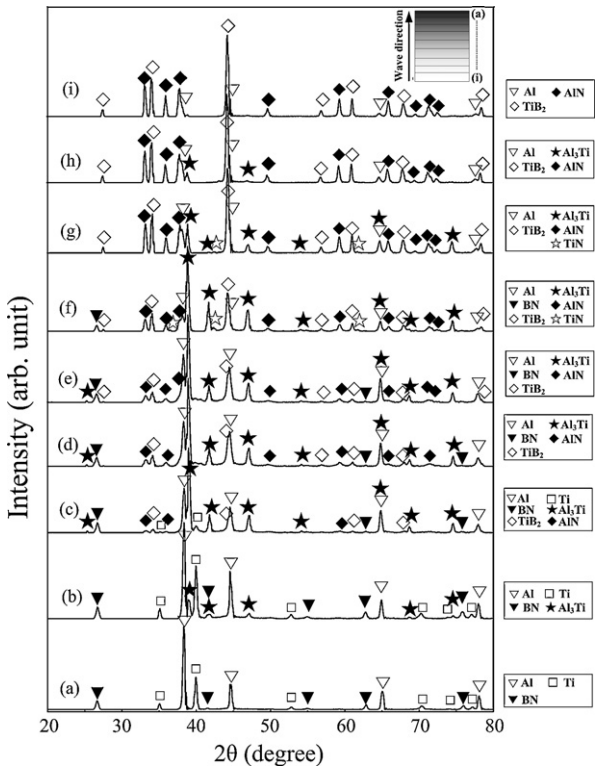

Fig. 6. X-ray microdiffraction patterns for the quenched 45 wt.% Al–Ti–BN sample in the differently reacted regions: (a) reactant region, (b → d) preheated region, (e → h) combustion region, and (i) reacted region.

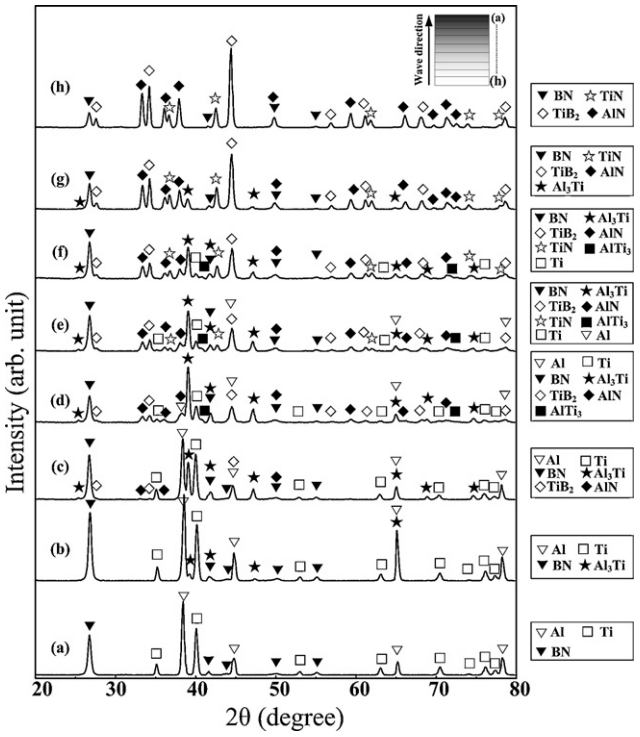

Fig. 7. X-ray microdiffraction patterns for the quenched 25 wt.% Al–Ti–BN sample in the differently reacted regions: (a) reactant region, (b → c) preheated region, (d → g) combustion region, and (h) reacted region.

$$\rightarrow \text{(f–g)Al} + \text{BN} + \text{Al}_3\text{Ti} + \text{AlN} + \text{TiB}_2 + \text{TiN} \rightarrow \text{(h)Al} + \text{BN} + \text{Al}_3\text{Ti} + \text{AlN} + \text{TiB}_2 \rightarrow \text{(i)Al} + \text{AlN} + \text{TiB}_2.$$

We can see that: (i) the Al_3Ti phase was priorly developed in the preheated region [Fig. 6(b)]; (ii) the AlN and TiB_2 phases had formed in the preheated region [Fig. 6(c) and (d)] before the elemental Al and Ti were completely consumed, while TiN had not. The formation of AlN and TiB_2 may result from the direct reaction between Al_3Ti and BN [*i.e.*, reaction (19)] or from the individual reactions between the elemental Al and BN and further of the resultant B or Al–B intermetallics/melt with Ti [*i.e.*, reactions (12) and (13)]. The nonsynchronous reactions are also likely to lead to the separate distribution of the AlN and TiB_2 phases; (iii) as the reaction proceeded, the elemental Al and Ti were greatly consumed, while the Al_3Ti, AlN and TiB_2 phases progressively increased [Fig. 6(c)–(f)]. The TiN phase appeared only after the elemental Ti was exhausted, suggesting that its formation may not result from the direct reaction between Ti and BN, but from the transient bonding of titanium (Ti) in the Al–Ti melt (note that the Al–Ti intermetallics in the reaction zone could be melted as the combustion wave arrived) with the nitrogen (N) atoms diffused away from the BN crystal; (iv) subsequently, the quantity of Al_3Ti substantially decreased while that of AlN, TiB_2 and the elemental Al increased; on the other hand, the transiently developed TiN phase vanished again, indicating that reactions (16) and (19) did take place, and the presence of excess Al in the reactants indeed inhibited the development of the TiN phase, which was in consistent with the previous thermodynamic prediction; (v) finally, in the reacted region, the product consisted of TiB_2, AlN, excess Al and a very small quantity of Al_3Ti, indicating a fairly complete reaction.

It is worthwhile to further emphasize that during the SHS reaction, the amount of the elemental Al first decreased and then increased, implying that most Al participated in the reaction through the formation of the Al_3Ti intermediate phase, whose amount first increased and then dramatically decreased. On the other hand, the consumption of a large amount of BN occurred only after the formation of considerable amount of Al_3Ti and depletion of the elemental Ti, suggesting that the reaction between Al_3Ti and BN was primary in the reaction zone and the reaction progress was essentially dictated by the rates of B and N dissociating from the BN body and then diffusing in the Al–Ti melt.

On the other hand, the reaction sequence in the 25 wt.%Al–Ti–BN quenched sample (Fig. 7) could be written as:

$$\text{(a)Al} + \text{Ti} + \text{BN} \rightarrow \text{(b)Al} + \text{Ti} + \text{BN} + \text{Al}_3\text{Ti} \rightarrow \text{(c–d)Al} + \text{Ti} + \text{BN} + \text{Al}_3\text{Ti} + (\text{AlTi}_3) + \text{AlN} + \text{TiB}_2 \rightarrow \text{(e)Al} + \text{Ti} + \text{BN} + \text{Al}_3\text{Ti} + \text{AlTi}_3 + \text{AlN} + \text{TiB}_2 + \text{TiN} \rightarrow \text{(f)Ti} + \text{BN} + \text{Al}_3\text{Ti} + \text{AlTi}_3 + \text{AlN} + \text{TiB}_2 + \text{TiN} \rightarrow \text{(g)Al}_3\text{Ti} + \text{AlN} + \text{TiB}_2 + \text{BN} + \text{TiN} \rightarrow \text{(h)BN} + \text{TiN} + \text{AlN} + \text{TiB}_2.$$

Compared with that in the high Al content sample, the reactions were similar in the initial stages, *i.e.*, the prior formation of Al_3Ti and then development of the AlN and TiB_2 phases, yet without appearance of TiN. This result clearly demonstrates that the formation of AlN had precedence over that of TiN, which appeared only in the reaction zone after the Al reactants were substantially consumed [Fig. 7(e)]. As the reaction advanced, the amount of TiN increased with the decrease in the elemental Ti, and simultaneously, that of AlN also increased [Fig. 7(d)–(g)]. Therefore, the outcome of a large amount of TiN should result from the direct reaction between Ti and BN, instead of that between Ti and AlN. Virtually, even in the 10 wt.%Al–Ti–BN sample, the amount of AlN also continuously increased through the reaction between the Al–Ti melt and BN. With the progress of the reaction, the Al–Ti melt was

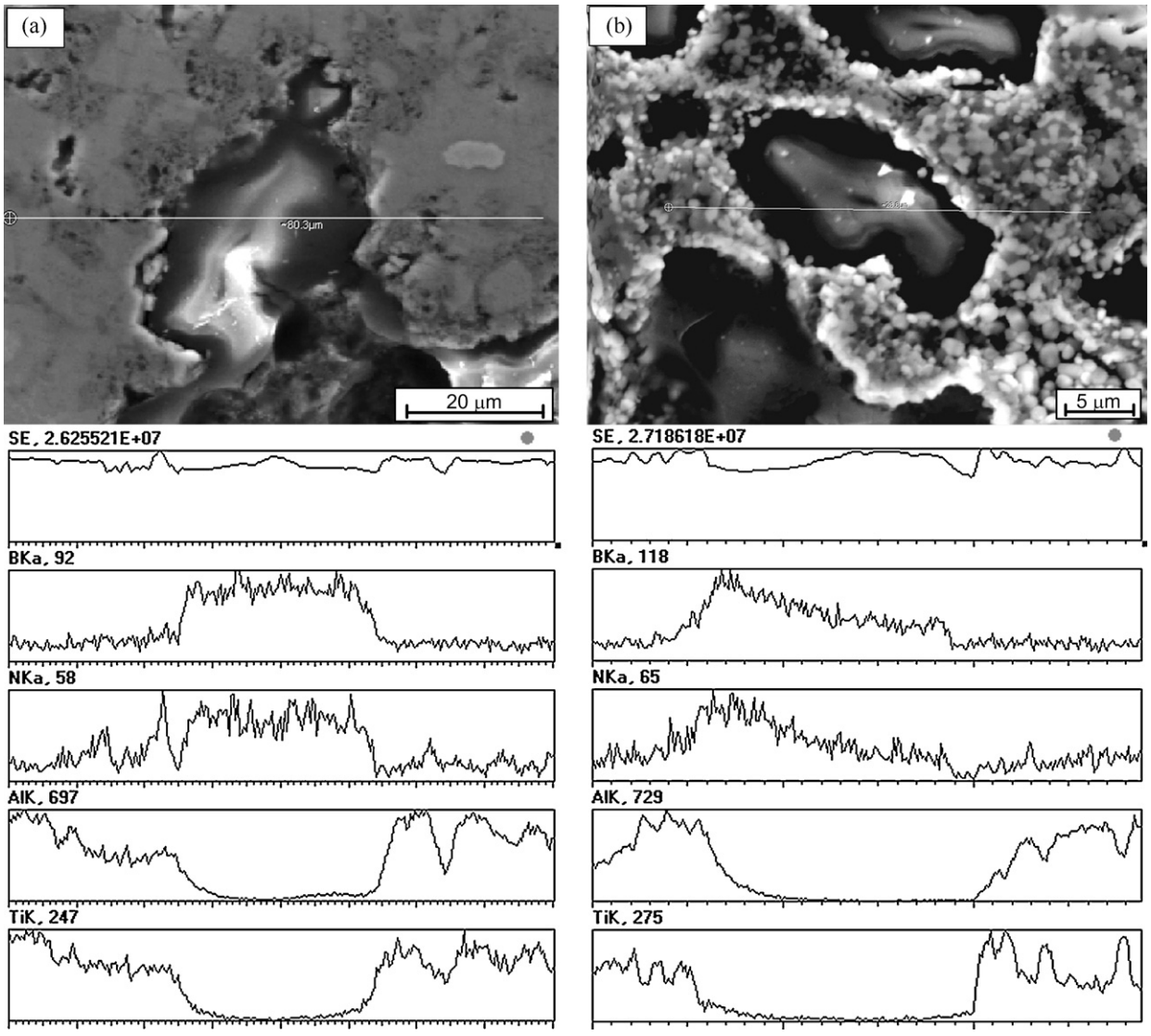

Fig. 8. Microstructures in the (a) preheated zone and (b) combustion zone of the quenched 45 wt.% Al–Ti–BN sample along with the elemental line spectra. Figure (a) shows that the BN particle was surrounded by the Al–Ti intermetallics and figure (b) shows that the remnant BN particles were surrounded by numerous fine ceramic particles with the gray ones being AlN and the bright ones being TiB_2. The elemental line spectra show the outward diffusion of B and N.

finally exhausted, and all the Al reactants transformed to AlN and the Ti to TiB_2 and TiN. The final product consisted of TiB_2, AlN, TiN and excess BN.

Accordingly, we deem that the reaction mechanisms, in a general sense, do not differ significantly in the Al–Ti–BN systems with low and high Al contents. The reactions in both cases commenced with the formation of Al_3Ti and then proceeded with the consumption of BN under the invasion of Al–Ti melt [see Fig. 8(a)]. The outward diffusion of B and N from the BN body to the surrounding Al–Ti melt yielded the AlN and TiB_2 phases [see Fig. 8(b)], releasing a large amount of heat and thus promoting the reaction. The difference in the high Al and low Al content samples was in the stage of formation of the TiN phase. In the high Al content samples, TiN could transiently develop through the bonding of the N atoms with the Ti atoms in the Al–Ti melt but was subsequently displaced by the excess Al into formation of AlN and Al_3Ti. Whereas, in the low Al content samples, TiN formed through the direct reaction between Ti and BN and could stably exist in the final product due to the deficiency in Al. As a result, the TiB_2–AlN-based composites consisting of binary or ternary ceramic phases with fine microstructures could be obtained by a proper manipulation of the Al content in the reactants.

4. Conclusions

(1) The Al content in the reactants has significant effects on the reaction behaviors and the phase compositions of the SHS product in the Al–Ti–BN system. The reaction exotherm and combustion wave velocity reach maxima at 35.5 wt.% Al. The final products consisting of TiB_2–AlN or TiB_2–AlN–TiN matrix composites could be selectively produced by a proper manipulation of the Al reactant content.

(2) The reaction mechanism in the Al–Ti–BN system during the SHS process is only moderately dependent on the Al reactant content. The primary reactions are the preferential formation of Al_3Ti and then reaction of the Ti–Al intermetallics/melts with BN. The substantial reaction between the elemental Ti and BN into formation of TiN takes place only in the low Al content samples.

(3) Formation of only TiB_2 and AlN phases is most thermodynamically feasible and exothermic in the 2Al–1Ti–2BN compacts. However, a slight excess of the Al reactant favors the elimination of the TiN phase in the product.

(4) The grain sizes of the resultant TiB_2, AlN and TiN phases as well as their distribution status are dependent on the Al reactant

content. Increasing the Al content promotes the grain growth and the separate residence of the AlN and TiB_2 phases. Whereas, the presence of TiN effectively inhibits the abnormal anisotropic growth of the TiB_2 grains.

Acknowledgements

This work is supported by the National Natural Science Foundation of China (No. 50531030) and the 4th Development Project for Talents in Jilin Province.

References

[1] B. Basu, G.B. Raju, A.K. Suri, Processing and properties of monolithic TiB_2 based materials, Int. Mater. Rev. 51 (2006) 352–374.
[2] C.L. Yeh, G.S. Teng, Use of BN as a reactant in combustion synthesis of TiN–TiB_2 composites under nitrogen pressure, J. Alloys Compd. 417 (2006) 109–115.
[3] X.Y. Zhang, S.H. Tan, D.L. Jiang, AlN–TiB_2 composites fabricated by spark plasma sintering, Ceram. Int. 31 (2005) 267–270.
[4] X.J. Zhang, Y.T. Zheng, J.C. Han, Low-pressure injection molding and SHS-HIP without envelope of AlN–TiB_2 ceramic slender tube with blind hole, Mater. Des. 26 (2005) 410–416.
[5] R. Tomoshige, A. Murayama, T. Matsushita, Production of TiB_2–TiN composites by combustion synthesis and their properties, J. Am. Ceram. Soc. 80 (1997) 761–764.
[6] F. Olevsky, P. Mogilevsky, E.Y. Gutmanas, I. Gotman, Synthesis of in situ TiB_2/TiN ceramic matrix composites from dense BN–Ti and BN–Ti–Ni powder blends, Metall. Mater. Trans. A 27A (1996) 2071–2079.
[7] M. Shibuya, M. Ohyanagi, Z.A. Munir, Simultaneous synthesis and densification of titanium nitride/titanium diboride composites by high nitrogen pressure combustion, J. Am. Ceram. Soc. 85 (2002) 2965–2970.
[8] L.H. Li, H.E. Kim, E.S. Kang, Sintering and mechanical properties of titanium diboride with aluminum nitride as a sintering aid, J. Eur. Ceram. Soc. 22 (2002) 973–977.
[9] S.V. Schneider, M. Desmaison-Brut, Y.G. Gogotsi, J. Desmaison, Oxidation behavior of a hot isostatically pressed TiB_2–AlN composite, Key Eng. Mater. 113 (1996) 49–58.
[10] K. Shobu, T. Watanabe, Y. Enomoto, K. Umeda, Y. Tsuya, Frictional properties of sintered TiN–TiB_2 and Ti(CN)–TiB_2 ceramics at high temperature, J. Am. Ceram. Soc. 70 (5) (1987) C-103–C-104.
[11] G.J. Zhang, Z.Z. Jin, Reactive synthesis of AlN/TiB_2 composites, Ceram. Int. 22 (1996) 143–147.
[12] E.Y. Gutmanas, I. Gotman, Dense high-temperature ceramics by thermal explosion under pressure, J. Eur. Ceram. Soc. 19 (1999) 2381–2393.
[13] B.L. Zou, P. Shen, Q.C. Jiang, Reaction synthesis of TiC–TiB_2/Al composites from an Al–Ti–B_4C system, J. Mater. Sci. 42 (2007) 9927–9933.
[14] L. Zhan, P. Shen, S.B. Jin, Q.C. Jiang, Combustion synthesis of Ti(C, N)–TiB_2 from a Ti–C–BN system, J. Alloys Compd. doi:10.1016/j.jallcom.2009.01.087.
[15] I. Barin, Thermochemical Data of Pure Substances, 3rd ed., Wiley-VCH Verlag GmbH, Weinheim, Germany, 1995.
[16] M.W. Chase Jr., C.A. Davies, J.R. Downey Jr., D.J. Frurip, R.A. McDonald, A.N. Syverud, JANAF Thermochemical Tables (3rd ed.), J. Phys. Chem. Ref. Data, vol. 14, Suppl.1, 1985.
[17] J.J. Moore, H.J. Feng, Combustion synthesis of advanced materials: Part I. Reaction parameters, Prog. Mater. Sci. 39 (1995) 243–273.
[18] Z.Q. Zhang, P. Shen, Y. Wang, Y.P. Dong, Q.C. Jiang, Fabrication of TiC and TiB_2 locally reinforced steel matrix composites using a Fe–Ti–B_4C–C system by an SHS-casting route, J. Mater. Sci. 42 (2007) 8350–8356.
[19] P. Shen, B.L. Zou, S.B. Jin, Q.C. Jiang, Reaction mechanism in self-propagating high temperature synthesis of TiC–TiB_2/Al composites from an Al–Ti–B_4C system, Mater. Sci. Eng. A 454–455 (2007) 300–309.
[20] D. Brodkin, S.R. Kalidindi, M.W. Barsoum, A. Zavaliangos, Microstructural evolution during transient plastic processing of titanium carbide–titanium boride composites, J. Am. Ceram. Soc. 79 (1996) 1945–1952.
[21] A.D. LeClaire, Diffusion of C, N, and O in metals, in: H. Mehrer (Ed.), Diffusion in Solid Metals and Alloys, LANDOLT-BÖRNSTEIN, New Series, III/26, Springer-Verlag, Berlin, 1990, pp. 485–486.
[22] T.B. Massalski, T.L. Murray, H.L. Bennett, H. Baker, Binary Alloy Phase Diagrams, American Society for Metals, Metals Park, Ohio, 1986.